Dávid Molnár, Árpád Veress

IMPLEMENTATION AND UTILIZATION OF INVERSE DESIGN METHOD FOR STATIC PRESSURIZE IN CASCADE

Todays, beside the continuously increasing scientific coverage of CAE[1], it is widely spread in the all fields of the industry. The basic reason of this is that significant cost, capacity and time can be saved by the simulation driven product development. The CFD[2] is a part of the CAE, and its effectiveness can be increased more by optimization algorithms. One of these technologies is the inverse design method, in which a predefined, in specific sense so called optimal flow condition has been imposed to recover the geometry belongs to that state. An inverse design method, developed at BME[3] Department of Aeronautics, Naval Architecture and Railway Vehicles, has been used in the present work for investigating the way of how the static pressurise and mass flow rate can be maximised in a cascade on such a way that the flow on the suction side of the profile to be close, but certain safe distance far from the separation. The effect of the blade pitch is also included in the present investigation.

Keywords: CFD, inverse design method, separation, optimization, cascade

INTRODUCTION

Computer modelling is used worldwide in different areas; many researches are in progress based on this technique [1][2][3][4]. In the past years, thanks to the advancement of the technology the computers achieved large computing capacity which made possible quick completion of huge number of calculations in short period of time. This made possible the development of numerical methods further.

CFD is a contribution of the CAE which uses numerical methods and algorithms to solve problem related to fluid mechanics. As a result the properties such as density, velocity, temperature and pressure of the flow can be predicted at any discretized points of the flow field. Nowadays the processes of industry, agriculture, defence, meteorology, environmental protection, space sciences and academia benefit the most.

In turbo machines with the help of this software, the properties of the flow and the emerging phenomena around a body can be studied. The opportunity is given to test the parts in a virtual environment, find missing or faulty elements which was not possible before. With these means time and cost can be saved, since the production of the optimized prototype is enough to test in practice.

The recent studies are aimed on the possibility to combine the CFD with optimization methods. At the moment the most of these methods require time and huge computing capacity, because the direct optimization methods for instance require big amount of computing results to determine the direction of the optimization and the change of the geometry. Furthermore the required number of flow solutions increase with the number of with the number of design variables [5].

---

[1] CAE: Computer Aided Engineering. Computer software used for engineering analysis tasks
[2] CFD: Computational Fluid Dynamics. A branch of fluid dynamics which uses numerical analysis to solve problems in fluid flow
[3] BME: Budapesti Műszaki és Gazdaságtudományi Egy. (Budapest University of Technology and Economics)

Nomenclature

Latin letters and symbols:

- ✈ c [m, m/s]   chord, sound speed;
- ✈ C_P [-]   pressure coefficient;
- ✈ $\overline{C_P}$ [-]   pressure coefficient;
- ✈ p [Pa]   pressure;
- ✈ M [-]   Mach-number;
- ✈ R [J/kg/K]   specific gas constant;
- ✈ u, v [m/s]   axial and tangential velocity component;
- ✈ a, b [-]   constant used in Stratford's formula;
- ✈ x [-]   distance from the leading edge;
- ✈ T [K]   temperature;
- ✈ U [-]   vector of conservative variables;
- ✈ F, G [-]   vector of inviscid fluxes;
- ✈ E [J/kg]   total energy;
- ✈ H [J/kg, -]   total enthalpy, numerical flux;
- ✈ W [m]   variables of the characteristic vector;
- ✈ V_n [m/s]   velocity, perpendicular to the cell face;
- ✈ t [s]   time;
- ✈ V_s [m/s]   velocity, parallel to the cell face;
- ✈ H_n [-]   normal directional flux;
- ✈ x, y [m]   Cartesian coordinates.

Greek letters:

- ✈ α [deg]   angle of attack;
- ✈ α_k [-]   Runge-Kutta constant;
- ✈ γ [-]   ratio of specific heats;
- ✈ μ [Ns/m^2]   dynamic viscosity;
- ✈ ν [m^2/s]   kinematic viscosity;
- ✈ ρ [kg/m^3]   density;
- ✈ Γ [m]   length of the cell's wall;
- ✈ Ω [m^2]   control area;
- ✈ $\lambda_n^{(I)}$ [m/s]   normal eigenvalues;
- ✈ Δ [-]   difference;
- ✈ π [-]   static pressure ratio.

Indexes:

- ✈ x, y axes (in the Cartesian coordinate system);
- ✈ 0 total parameters;
- ✈ 1 flow parameters;
- ✈ $n+1$ wall adjacent characteristic in the next time step;
- ✈ $n-1$ wall adjacent characteristic in the previous time step;
- ✈ $*$ wall adjacent extrapolated parameters from the interior;
- ✈ i, j spatial variables;

✈ *in, out*   inlet, outlet;
✈ *l*   local variables;
✈ *m*   values for the location of the pressure increase's start;
✈ *n*   variables perpendicular to the wall;
✈ *o*   initial parameters;
✈ *to, stat*   total, static;
✈ *∞*   parameters at infinite far from the investigated point.

Abbreviations:
✈ BC   Boundary Conditions;
✈ PBC   Physical Boundary Conditions;
✈ NBC   Numerical Boundary Conditions;
✈ MBC   Mirror Boundary Conditions;
✈ CAE   Computer Aided Engineering;
✈ CFD   Computational Fluid Dynamics;
✈ MUSCL   Monotone Upstream Schemes for Conservation Laws;
✈ L   left side of cell's face;
✈ R   right side of cell's face;
✈ Re   Reynolds-number;
✈ RK   Runge-Kutta;
✈ ss, ps   suction side, pressure side.

Inverse Design for Aeronautical Applications

During the inverse design method, the modification of the starting geometry is based on a set of pre-defined variables. These methods are become more attractive amongst other optimization methods because of the used fast and robust algorithms. The wall modification requires less flow solutions for inverse design than other optimization techniques. Hence, the required computer resources are lower and the inverse design is very innovative to be used in practice. However, the drawback of this method is that a goal pressure or velocity distribution must be given, which the solution of the inverse design method will correspond with. It can be difficult to define these expected distributions which will satisfy all design goals. One cannot guarantee that the prescribed distribution will not result in a mechanically wrong, unachievable geometry where the geometry intersects itself. Also even if the geometry is acceptable the outlet edges thickness can be zero, or can stay open which is not achievable in practice.

The iterative procedure of the inverse design method, at first, requires an initial geometry and a required pressure/velocity distribution along the wall to be modified. The method will modify this geometry until it reaches the goal pressure/velocity distribution. The prescribed distribution can be the goal function of an optimization technique or a solution of an industrial experience or theory for example. The iterative cycle starts with a direct analysis of the inviscid Euler solver in the present case on the initial geometry. Upon completing the convergence criteria if the target conditions are not met, new boundary condition is defined at the solid boundary to be inverse designed. The wall become open locally as inlet or outlet depends on the pressure difference between the boundary and the computational domain. The outcome is a velocity distribution along the wall which does not necessarily parallel with it. The final step of the iterative

cycle is that the wall become parallel with the local velocity vector corresponds to the new streamline of the flow field. These steps are repeated until the target distribution reached and the new geometry is available [6].

The one of the key points in fluid dynamic related engineering phenomena is that the flow may/should close, but certain distance far from the separation to minimize the losses meanwhile it is distorted as much as possible to reach design specifications if it is the case. Hence, the methods for predicting separation are described in the following chapter to be considered afterwards in the inverse design method.

SEPARATION PREDICTION METHODS

There are several existing methods for predicting separation as Goldschmied, Stratford, Head, Cebeci-Smith for instance. The accuracies of these models were studied several times. Investigations show that the operation of Goldschmied method is unreliable in certain cases, while the other three leads to similar results. The method of Stratford, Head and Cebeci-Smith are acceptable and the Cebeci-Smith is the most accurate followed by Head's method. However, Stratford's predicts the separation slightly early. Due to the suitable accuracy, robustness, simplicity and representing "the worst case" condition, Stratford method was used to determine the pressure distribution during the inverse design in the present case. The base of the Stratford method is to determine a positive pressure gradient where the boundary layer to be close, but certain safe distance far from the separation [6].

Stratford's Separation Prediction Method

A suction side pressure distribution of an airfoil is shown in Fig. 1. The pressure decreases until the x_0 point where the pressure increase starts. The pressure needs to increase until it reaches the pressure value at the trailing edge of the pressure side.
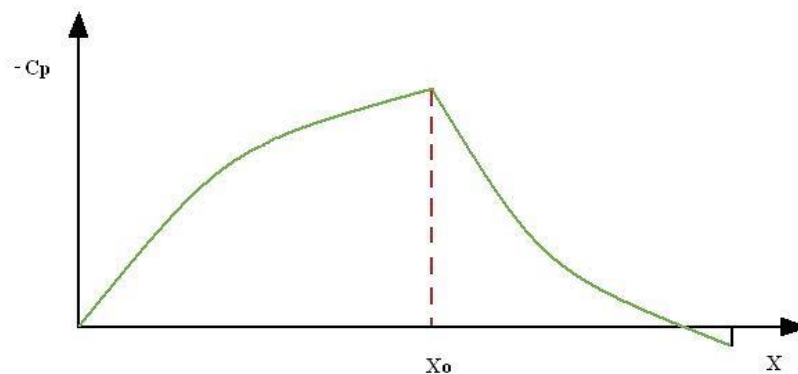

Figure 1. Pressure distribution over the equivalent Stratford plate [8]

In the Stratford's simplified model the static pressure section is followed by the pressure increase from the x_0 point as it is shown in Fig. 2.
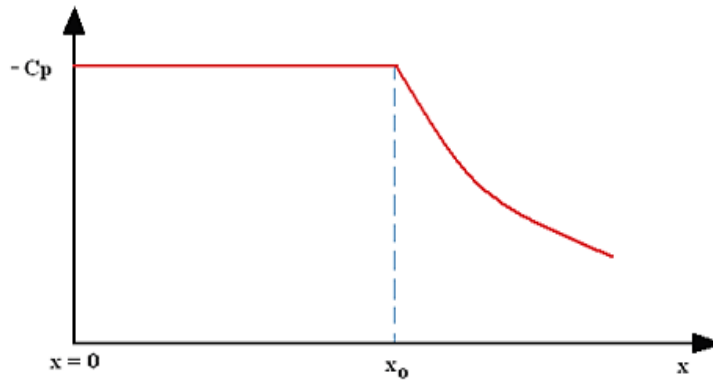
Figure 2. Stratford's simplified view of the front of the airfoil [8]

Stratford derived an empirical formula by measurement over a flat plate to predict the point of the separation in an arbitrary decelerating flow at around the Reynolds-number range 10E6 [12]:

$$\frac{\overline{C}_p\left[x\left(d\overline{C}_p/dx\right)\right]^{1/2}}{\left(10^{-6}\,Re\right)^{1/10}} = S \tag{1}$$

Where the canonical pressure distribution is the following [13]:

$$\overline{C}_p = \frac{p - p_0}{\frac{1}{2}\rho_0 u_0^2} \tag{2}$$

if $\dfrac{d^2 p}{dx^2} \geq 0$ then $S=0.39$ or if $\dfrac{d^2 p}{dx^2} < 0$ then $S=0.35$ and $\overline{C}_p < \dfrac{4}{7}$. x is the distance measured from the leading edge of the flat plate and:

$$Re = \frac{u_0 x}{\nu} \tag{3}$$

To calculate the dynamic viscosity Sutherland's method was used [14]:

$$\mu = \frac{C_1 T^{3/2}}{T + S} \tag{4}$$

where $C_1 = 1.458 \cdot 10^{-6}\ \dfrac{kg}{ms\sqrt{K}}$ and $S = 110.4\ K$.

If in the flow the pressure rise begins at the point x_0 (where the pressure is minimal and the velocity is maximal and the 0 is the subscript of the parameters belongs to that condition) the equations (1) left-hand side starts from a zero value and grows continuously. When S limiting values is reached the separation occurs.

If S is held at the limiting value of 0.39, then equation (1) forms an ordinary differential equation for $\overline{C}_p(x)$. Equation (1) shows that the flow described by it is ready to separate on every point. The solution for equation (1) presented by Stratford follows [12]:

$$\overline{C}_p = 0.645\left\{0.435\,Re_0^{1/5}\left[\left(x/x_0\right)^{1/5} - 1\right]\right\}^{2/n} \quad if \quad \overline{C}_p \leq (n-2)/(n+1) \tag{5}$$

and

$$\overline{C}_p = 1 - \frac{a}{\left[(x/x_0) + b \right]^{1/2}} \quad if \quad \overline{C}_p \geq (n-2)/(n+1).$$ (6)
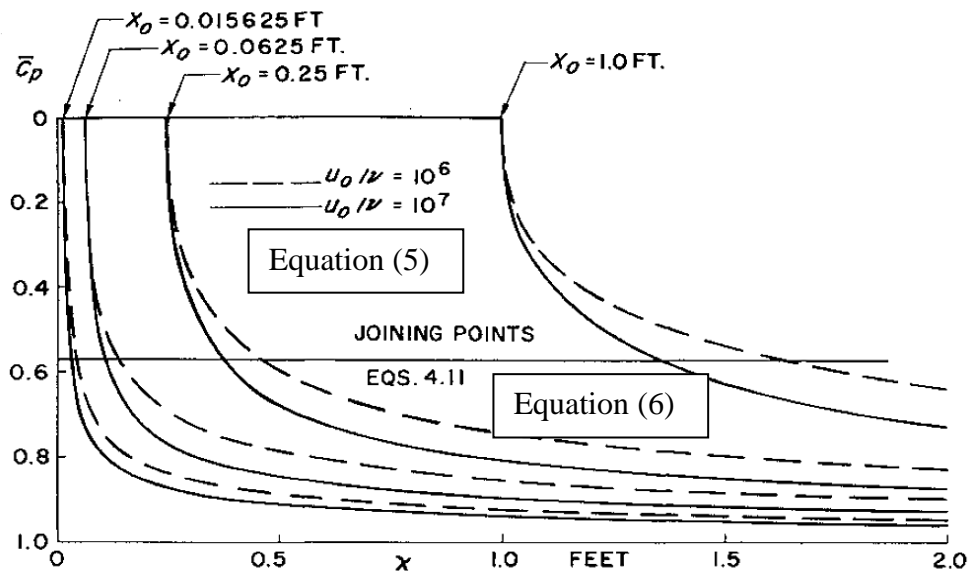

Figure 3. Stratford limiting flows at two values of unit Reynolds number [12]

In this two-part solution, x_0 is the location of the start of the pressure increase, $Re_0 = \frac{u_0 x_0}{\nu}$, x is the distance from the start of the flow, which starts as a turbulent flow over the wall. The value of "n" is defined as 6 by Stratford.

In the equation a and b are constants values and required so the steepness of the two curves match in the connection point.

Equation (5) describes the first section of the flow while equation (6) describes the second. The above said two equations were computed and shown.

The actually presented method is used for the determination of pressure distribution at maximum lift force for given far field conditions. The following equation is applied to determine the integral of the pressure distribution around the profile [13]:

$$\aleph\left(\overline{C}_p(x) \right) = \Im\left(C_p(x) \right) = \oint C_p(x)dx = \oint \frac{p - p_\infty}{\frac{1}{2}\rho_\infty u_\infty^2} dx = \oint \frac{p - p_\infty}{0.5\gamma p_\infty M_\infty^2} dx$$ (7)

where p is the static pressure at the given location of the wall and the other variables are correspond to the free stream conditions (far upstream (total temperature and pressure) and far downstream (static pressure) of the cascade). The connection between $\overline{C}_p(x)$ and $C_p(x)$ is given by equation (8) [13].

$$\overline{C}_p = \frac{p-p_0}{\frac{1}{2}\rho_0 u_0^2} = \frac{C_p - C_{p,0}}{1 - C_{p,0}} = \frac{\dfrac{p-p_\infty}{\frac{1}{2}\rho_\infty u_\infty^2} - \dfrac{p_0 - p_\infty}{\frac{1}{2}\rho_\infty u_\infty^2}}{1 - \dfrac{p_0 - p_\infty}{\frac{1}{2}\rho_\infty u_\infty^2}} = \frac{p-p_0}{p^{total} - p_0} = \frac{p-p_0}{\frac{1}{2}\rho_0 u_0^2} \tag{8}$$

The pressure coefficient at the minimum pressure (p_0) is given by:

$$C_p = C_{p,0} = \frac{p_0 - p_\infty}{\frac{1}{2}\rho_\infty u_\infty^2} = \frac{p_0 - p_\infty}{0.5\gamma p_\infty M_\infty^2} = \frac{p_0 - p_\infty}{0.7 p_\infty M_\infty^2} \tag{9}$$

where p_0 and maximum velocity u_0 are constants from the leading edge of the suction side until the start of the positive pressure gradient. The M_0 Mach number is calculated by:

$$C_p = C_{p,0} = \frac{p_0 - p_\infty}{0.7 p_\infty M_\infty^2} = \frac{1}{0.7 M_\infty^2}\left[\left(\frac{1+0.2 M_\infty^2}{1+0.2 M_0^2}\right)^{\frac{\gamma}{\gamma-1}} - 1\right] \tag{10}$$

T_0, ρ_0 and u_0 are obtained by the energy equation of the isentropic flow and ideal gas law:

$$T_0 = T^{total}\left(1 + \frac{\gamma-1}{2} M_0^2\right)^{-1} \tag{11}$$

$$u_0 = \sqrt{\frac{\gamma}{\gamma-1} R\left(T^{total} - T_0\right)2} \tag{12}$$

$$\rho_0 = \frac{p_0}{RT_0} \tag{13}$$

The total quantities correspond to the given operational and inlet (far field) boundary conditions. The way to determine pressure distribution starts with specifying a p_0. The parameters belongs to that p_0 can be calculated from the equations (10)–(13) with using static downstream pressure for determining M_∞. Next step is to find x_0 which gives back the required pressure at the trailing edge with the use of Stratford's equations (5) and (6). Stratford's limiting pressure distribution till the required pressure on the trailing edge of the blade is the output of the procedure [8].

THE DASFLOW

The DASFLOW is an in-house Euler solver developed at BME, Department of Aeronautics, Naval Architecture and Railway Vehicles. This software is used in the present investigation for numerical flow modelling.

Governing Equations

The unsteady 2D compressible Euler equations in Cartesian coordinate system have been considered for the mathematical model for the fluid dynamics:

$$\frac{\partial U}{\partial t} + \frac{\partial F(U)}{\partial x} + \frac{\partial G(U)}{\partial y} = 0 \tag{14}$$

where $x, y \in \Re$ and $t \in \Re^+$. The conservative variables and convective fluxes are given by:

$$U = \begin{pmatrix} \rho \\ \rho u \\ \rho v \\ \rho E \end{pmatrix}, F(U) = \begin{pmatrix} \rho u \\ \rho u^2 + p \\ \rho uv \\ \rho uH \end{pmatrix}, G(U) = \begin{pmatrix} \rho v \\ \rho vu \\ \rho v^2 + p \\ \rho vH \end{pmatrix} \tag{15}$$

The ρ is the density, u and v are velocity in Cartesian coordinate system and p is the static pressure. The total enthalpy and energy are given by (16).

$$H = \frac{\gamma}{\gamma - 1} \frac{p}{\rho} + \frac{u^2 + v^2}{2}, E = \frac{1}{\gamma - 1} \frac{p}{\rho} + \frac{u^2 + v^2}{2} \tag{16}$$

The γ is the ratio of specific heats [7].

Boundary Conditions

The numerical treatment of the boundary conditions influences the convergence properties and the accuracy of the results in solving partial differential system of equations. In case of a hyperbolic equations, if Ne is the number of partial differential equations and Np < Ne is number of Physical Boundary Conditions (PBC), then Nn = Ne–Np Numerical Boundary Condition (NBC) needs to be defined for the system to be well posed. The PBC grants the existence and the unicity of the solution while the NBC grants the exit of the perturbations from the system without reflection. For these reasons the correct combinations of the NBC and PBC should be used [13].

The simplified characteristic form of the governing equations can be expressed by the outward pointing normal components of the computational cell as follows [7]:

$$\frac{\partial W_n^{(1)}}{\partial t} + V_n \frac{\partial W_n^{(1)}}{\partial n} = 0;$$

$$\frac{\partial W_n^{(2)}}{\partial t} + V_n \frac{\partial W_n^{(2)}}{\partial n} = 0;$$

$$\frac{\partial W_n^{(3)}}{\partial t} + (V_n + c)\frac{\partial W_n^{(3)}}{\partial n} = 0$$

$$\frac{\partial W_n^{(4)}}{\partial t} + (V_n - c)\frac{\partial W_n^{(4)}}{\partial n} = 0; \tag{17}$$

Where n is the unit vector perpendicular to the computational cell's wall, V_n is the component of the velocity vector perpendicular to the cell wall, W_n is the characteristic variable into the direction n (the invariants of the Riemann equation) and (c) is the speed of sound. The W_n

invariants are constants on their characteristic curves. The direction of the characteristic curves, the direction of wave propagation (V_n, V_n, V_n+c, V_n-c) dependent of the V_n and the local speed of sound. On the boundaries, the number of the PBC is equal to the number of the negative eigenvalues. These conditions correspond to the input characteristics from the outside of the computational domain. The NBC becomes necessary because for the actual problem solving, conservative variables are used instead of Riemann variables. The general practice is to compute the incoming Riemann invariants by the PBCs meanwhile the outgoing ones are extrapolated from the interior of the computational domain.

The detailed description of the inlet outlet solid wall boundary conditions in theoretical manner are found in [13].

Discretization

Integrating system equation (14) over a control volume Ω which is bounded by interface Γ and applying the Gauss' divergence theorem gives [7]:

$$\frac{d}{dt}\iint_{\Omega} U d\Omega + \int_{\Gamma} \vec{H}\vec{n} d\Gamma = 0 \tag{18}$$

where n is the local outward pointing unit normal vector. $\vec{H} = F\vec{e}_x + G\vec{e}_y$ and $\vec{H}\vec{n}$ can be described as:

$$H_n = \vec{H}\vec{n} = \begin{pmatrix} \rho V_n \\ \rho u V_n + p n_x \\ \rho v V_n + p n_y \\ \rho V_n H \end{pmatrix} \tag{19}$$

where

$$V_n = \vec{V}\vec{n} = \left(u\vec{e}_x + v\vec{e}_y\right)\left(n_x\vec{e}_x + n_y\vec{e}_y\right) \tag{20}$$

Finite volume method was used to achieve a discrete form. The second integral in (18) can be replaced with the summation over the number of faces N_f of the control volume $\Omega_{i,j}$. The semi-discreet from of eq. (18) can be written for the cell j:

$$\frac{d}{dt}U_j = -\frac{1}{\Omega_j'}\sum_{k=1}^{N_b}[H_n]_{j,k}\Gamma_{j,k}' = \Re_j \tag{21}$$

where, $[H_n]_{j,k}$ is the total inviscid flux normal to the cell interface. U_j is the vector of the conservative variables. $\Gamma_{j,k}'$ is the length of the wall k belongs to cell j. During discretization the value of $[H_n]_{j,k}$ can be characterized with a flux function: $\hat{H}_n$ which takes into consideration the sign of the Jacobi matrices, in other words the relevant propagation directions:

$$\hat{H}_n\left(U^L, U^R\right) \tag{22}$$

The functions $\hat{H}_n\left(U^L, U^R\right)$ can be calculated by a special averaging of the left and right states of the cell face [13]:

$$\hat{H}_n\left(U^L, U^R\right) = \frac{1}{2}\left\{H_n\left(U^L\right) + H_n\left(U^R\right) - \left|\hat{D}_n\left(U^L, U^R\right)\right|\left(U^R - U^L\right)\right\} \tag{23}$$

In ideal gas – based on Roe's work – $\hat{D}_n$ matrix equals with the Jacobi matrix, when it is expressed as a function of $\hat{\rho}$, $\hat{u}$, $\hat{v}$, and $\hat{h}_0$ variables. These variables are weighted values with the square root of the density.

Roe's approximation method is less dissipative and closely linked with the characteristic transport, therefore this is one of the most effective Riemann-solver. It has an excellent discontinuity-capturing property including shear waves. However, this flux can produce non-physical expansion shocks, which violates the entropy conditions. This can be avoided by modifying the eigenvalues of the nonlinear fields based on Yee, as it is applied in the present case [13].

MUSCL (Monotone Upstream Schemes for Conversation Laws) approach is used for higher order spatial discretisation. It means a linear or higher order approximation of the conserved variables over the cell instead of constant ones. The mathematical representation starts with the Taylor-series expansion around the point i [13]:

$$U(x) = U_i + \frac{\partial U}{\partial x}\Big|_{x_i}(x - x_i) + \frac{1}{2}\frac{\partial^2 U}{\partial x^2}\Big|_{x_i}(x - x_i)^2 + O\left(\Delta x^3\right) \tag{24}$$

x is the spatial direction equals with the local coordinate in every direction. After discretization and integration the following equations can be written:

$$\overline{U}^R_{i+\frac{1}{2}} = U_{i+1} - \frac{1}{4}\left[(1-\kappa)\Delta_{i+\frac{3}{2}} + (1+\kappa)\Delta_{i+\frac{1}{2}}\right]$$

$$\overline{U}^L_{i+\frac{1}{2}} = U_i + \frac{1}{4}\left[(1-\kappa)\Delta_{i-\frac{1}{2}} + (1+\kappa)\Delta_{i+\frac{1}{2}}\right] \tag{25}$$

where

$\Delta_{i-\frac{1}{2}} = U_i - U_{i-1}$, $\Delta_{i+\frac{1}{2}} = U_{i+1} - U_i$ and $\Delta_{i+\frac{3}{2}} = U_{i+2} - U_{i+1}$ where, in the cell between the i-th and $(i+1)$-th points, the left and right side conditions exactly at the cell boundary are marked with L: Left and R: Right.

The $\kappa = 1/3$, which corresponds to the third order spatial accuracy of the 1 dimensional problem. In case of higher order discretization schemes, non-physical oscillation can appear in the solution because of the shock wave, discontinuity and sudden changes. Mulder limiter has been used in the present case to preserve the monotonicity of the scheme [13]:

$$\overline{U}^R_{i+\frac{1}{2}} = U_{i+1} - \frac{1}{4}\psi^R\left[\left(1 - \kappa\psi^R\right)\Delta_{i+\frac{3}{2}} + \left(1 + \kappa\psi^R\right)\Delta_{i+\frac{1}{2}}\right] \tag{26}$$

$$\overline{U}^L_{i+\frac{1}{2}} = U_i + \frac{1}{4}\psi^L\left[\left(1 - \kappa\psi^L\right)\Delta_{i-\frac{1}{2}} + \left(1 + \kappa\psi^L\right)\Delta_{i+\frac{1}{2}}\right] \tag{27}$$

To solve the equation above the non-linear, multi-step time integration method is used based on Runge-Kutta (RK). The advantage of the method is that the solution is achieved with the least computational cost with high stability. The *4th* ordered Runge-Kutta method is applied here to determine the time derivatives of the conservative variables.

The detailed description of the finite volume method is found in [9] and the analysis of the numerical method is described in [10].

The Wall Modification Method

The last step of the inverse iteration cycle is the modification of the geometry. The velocity distribution is given as an output of the permeable or opening wall based direct analyses. In the new position, the wall is set to be parallel with the local velocity vector by moving the coordinates only in y direction [6]:

$$\Delta y_i(x_i) = \sum_{k=Le}^{i} \left(\frac{v_k}{u_k} \Delta x_k \right) \tag{28}$$

u and v are the components of the velocity vector in the Cartesian coordinate system (see Figure 4). The wall modification starts from the leading edge till the trailing edge. [6]
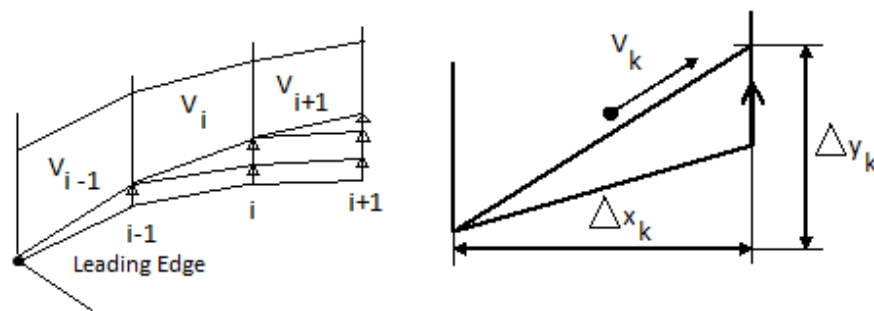
Figure 4. Schematic of the wall modification process based on the local velocity vector [13]

For the invers design's wall-modification, pressure or velocity distributions are required. Hereinafter the goal is to determine a pressure distribution from Stratford's method, which can be used in inverse design to optimize a blade profile in a cascade.

IMPLEMENTATION OF STRATFORD'S METHOD

The goal of this investigation is to define the optimal pressure distribution where the static pressurise and the mass flow rate over the cascade is maximal. For this purpose Stratford's method was used, which was described previously.

The Stratford's method was implemented in an Excel table. It was selected as an initial computational environment, because every step can be observed and any possible error become visible immediately. Concerning the conditions for the application of Stratford's method, the flow is supposed to be incompressible, boundary layer is turbulent and the Re is 10^6-10^7. At the start of the process the input table needs initial parameters such as the total pressure (p_{to}) and temperature (T_{to}) at the upstream of the blade row, static pressure at the downstream of the cascade

and the pressure coefficient (C_P). Then the static parameters ($Re_0, p_0, M_0, T_0, \rho_0$ and u_0) are calculated by the Excel.

Afterwards the points of the geometry (x) over the suction side are defined from the leading edge towards the trailing edge. In the following step the location of the pressure increase have to be defined (x_0). Hence, first, the value of (x_0) must be shifted - with sufficient accuracy - so that the pressure on the trailing edge will equal with the expected outlet static pressure downstream of the cascade. The Excel then calculates the canonical pressure coefficient from Stratford's equations. Finally the pressure and pressure coefficient are determined in every point.

The following equations describe the steps to determine the "*a*" and "*b*" constants for the canonical pressure distribution:

Eq. (5) when $n = 6$:

$$\frac{4}{7} = 0.645 \cdot \left\{ 0.435 \cdot \mathrm{Re}_0^{1/5} \left[(x/x_0)^{1/5} - 1 \right] \right\}^{2/6} \tag{29}$$

in term of (x)

$$x = \left(\left(\frac{4}{7 \cdot 0645} \right)^3 \cdot \frac{1}{0.435 \mathrm{Re}_0^{1/5}} + 1 \right)^5 x_0 \tag{30}$$

Differentiating eq. (5) and (6) with respect to (x):

$$\frac{d\overline{C}_p}{dx} = \frac{2 \cdot 0.645 \cdot \left(0.435 \mathrm{Re}_0^{1/5} \right)^{1/3} \left[(x/x_0)^{1/5} - 1 \right]^{2/6-1}}{6 \cdot 5 x_0 (x/x_0)^{4/5}} \quad \text{and} \tag{31}$$

$$\frac{d\overline{C}_p}{dx} = \frac{a}{2 x_0 (x/x_0 + b)^{3/2}} \tag{32}$$

In the Excel table:

$$x = A$$

$$K = 0.645 \cdot \left(0.435 \mathrm{Re}_0^{1/5} \right)^{1/3}$$

$$B = \frac{\left[(x/x_0)^{1/5} - 1 \right]^{-2/3}}{15 \cdot x_0 (x/x_0)^{4/5}} \tag{33}$$

$$a = 0.645 \cdot 0.435^{1/3} \cdot \left(\frac{A}{x_0 + b} \right)^{1/2}$$

$$b = \frac{0.645 \cdot 0.435^{1/3}}{2 \cdot B \cdot x_0} - \frac{A}{x_0}$$

With more pressure coefficient an array of curves are given to the same trailing edge pressure.

The final step is to determine which curve has the largest closed area. It is the optimal suction side pressure distribution due to the largest work on the flow.

The block diagram of the calculation process for one *Cp* is found in Figure 5. With the settings of initial input parameters different conditions can be considered and the length of the profile's chord can be set to a preferred value.
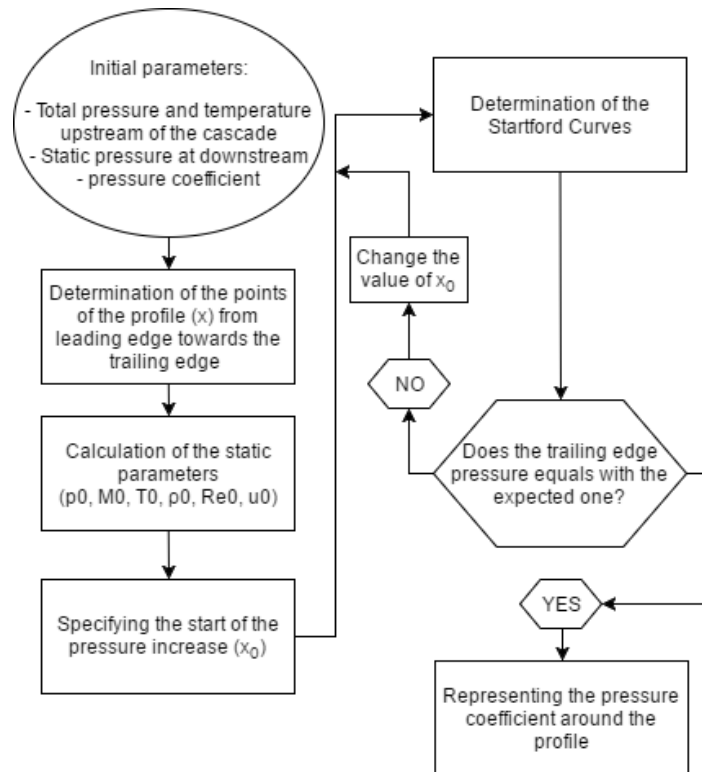

Figure 5. The process of determining the pressure distribution for one C_p

In the future a program can be written to speed up the iteration process and find the location of the pressure increase with better accuracy.

The array of pressure distribution curves with the inlet total pressure 107,853 Pa, inlet total temperature 298.42 K and static outlet (trailing edge) pressure 101,325 Pa is shown in Figure 6. The pressure coefficients are in the range of [−2.5, −0.5]. The curve with the largest area under it is coloured red.
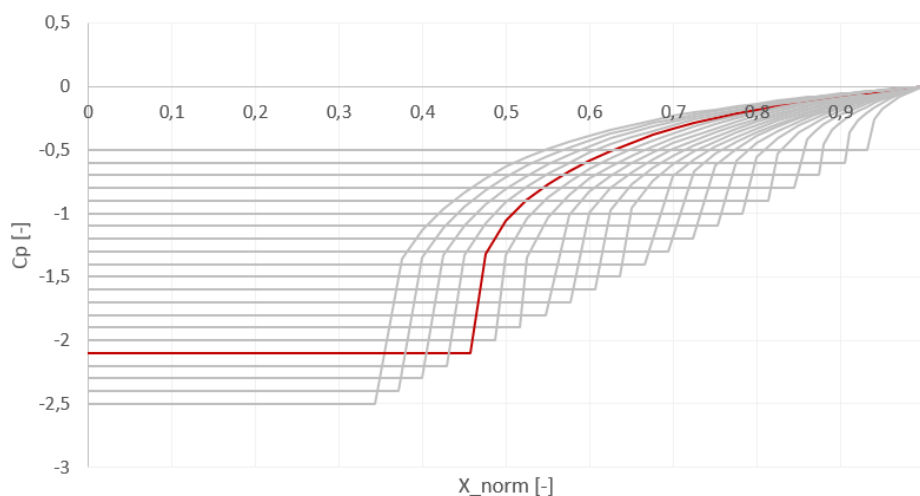
Figure 6. The pressure distribution for different pressure coefficients

EVALUATION OF THE RESULTS

Comparison of profiles with different pressure distribution

For comparison three different pressure distributions was selected. The curve with the largest area which in theory is the optimal pressure distribution for the inverse design and as a result will redirect the flow towards axial direction with the best efficiency is $C_p=-2.1$. The other two pressure distributions belongs to one of the lowest $C_p=-2.5$ and highest feasible pressure coefficient $C_p=-0.6$.

For initial parameters as mentioned in the previous chapter are: $p_{to} = 107,853\,Pa$ total pressure, $T_{to} = 298.42\,K$ total temperature, $p = 101,325\,Pa$ trailing edge static pressure. The flow angle (with respect to the horizontal direction) is $\alpha = 45° = 0.785398163\,rad$ in the present investigation.

The results of the inverse design method are discussed in the following subchapters.

Test Scenario $C_p = -0.6$
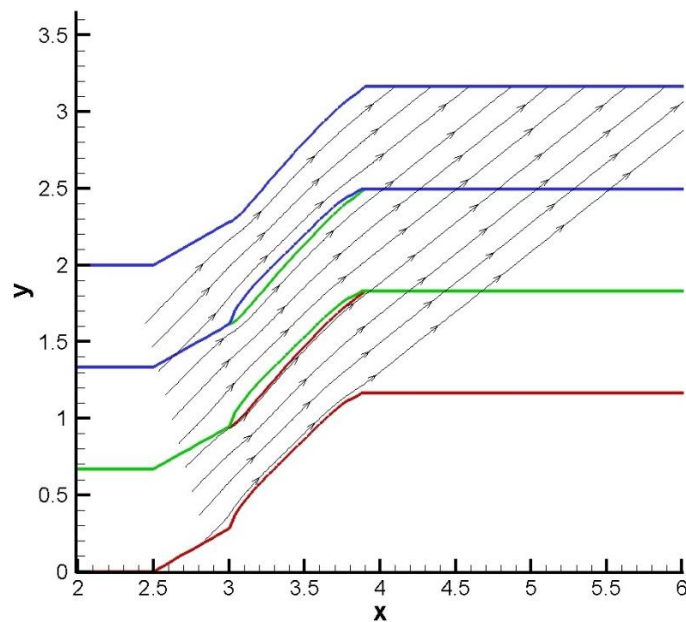
Figure 7. Streamlines over cascade at $Cp = -0.6$

Regarding the results at $C_p = -0.6$, the flow was redirected minimally the angle from the axial direction is 38.66° (see Figure 7). The mass flow rate is: 90.44 $kg/s^2/m$.
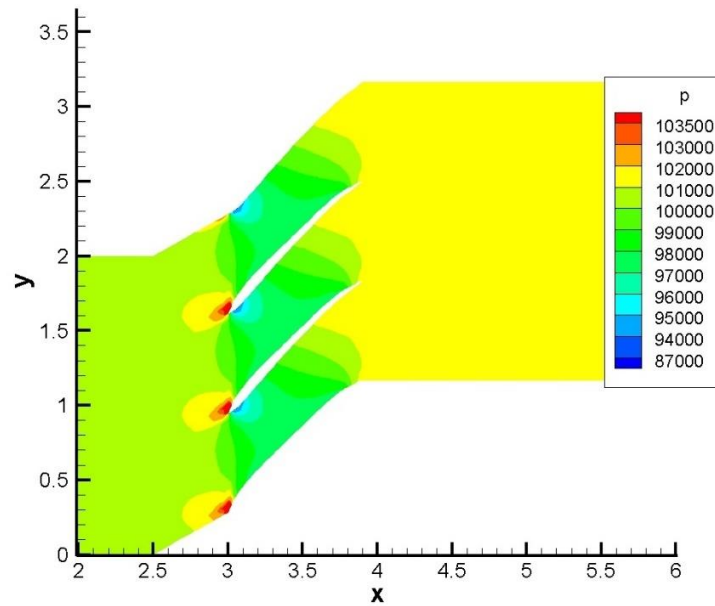
Figure 8. Pressure distribution over cascade at $C_p = -0.6$

The pressure increase is smallest among the investigated cases. The inlet static pressure is $p_{in} = 100,869 Pa$ (see Figure 8). The static pressure rise in this case is $\pi = 1.00454$. The low-range pressure zone on the suction side is large. With this kind of properties the pressure increases rather at the last section of profile which is due to the slightly negative angle of attack also. The Mach number distribution is shown in Figure 9. which confirms also the low level diffusivity.
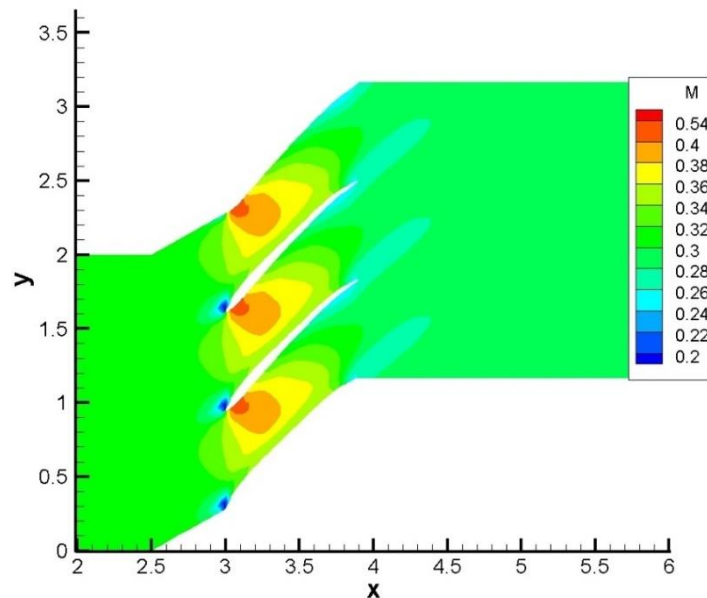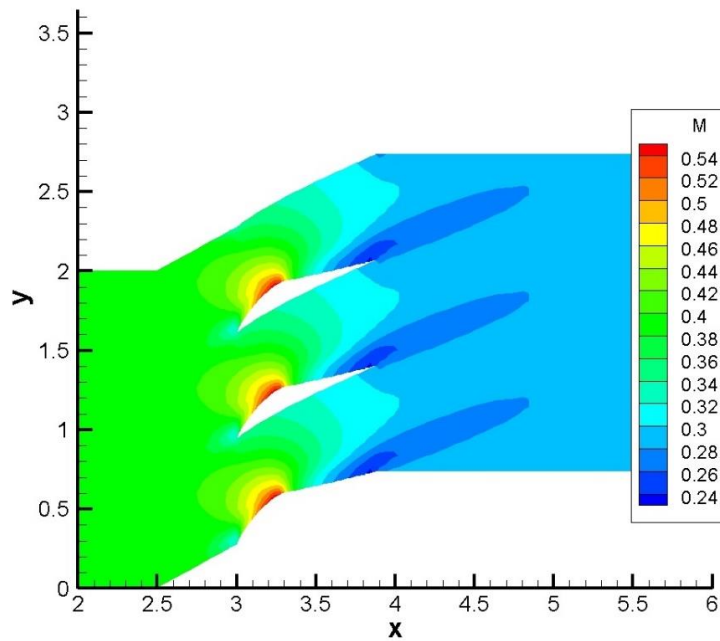

Figure 9. Mach-number distribution over cascade at $C_p = -0.6$

Test Scenario C$_p$ = −2.5
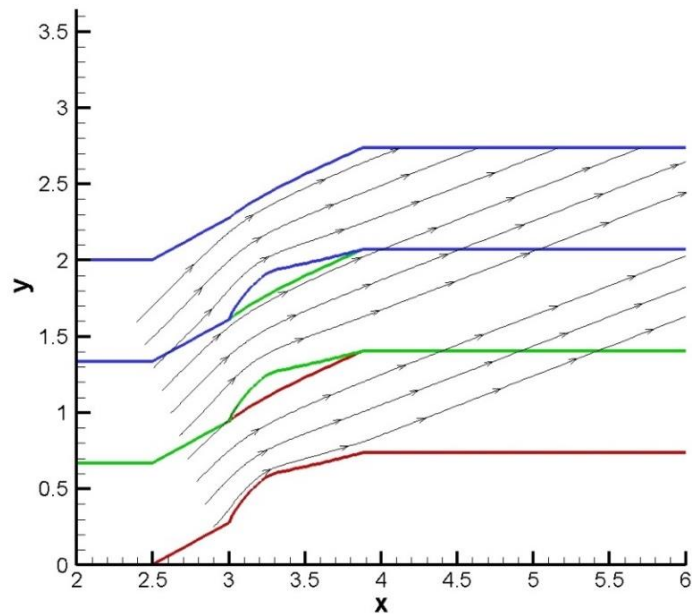
Figure 10. Streamlines over the cascade at $C_p = -2.5$

Closing towards the optimal pressure distribution the flow was more redirected, this is the result of the thickened profile and larger curvature (see Figure 10). The direction of the flow at the exit of the cascade measured from axial direction is 21.37°.
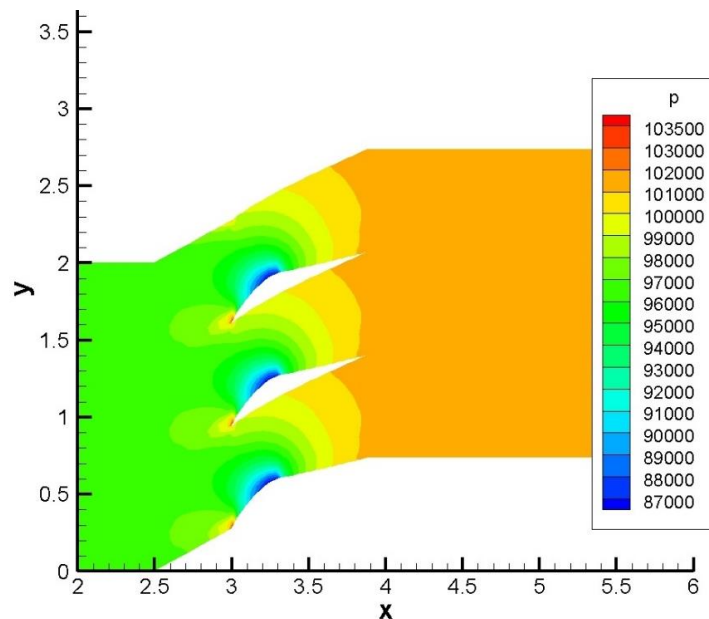
Figure 11. Pressure distribution over cascade at $C_p = -2.5$

The mass flow increased to: $110.72 kg/s^2/m$. The static pressure increases more, it is $p_{in} = 96,925 Pa$. The static pressure rise in this case is $\pi = 1.0454$ (see Figure 11). The low-range pressure zone is the smallest between the investigated cases. This design uses the largest part of the profile, because the start of the pressure increment here starts the earliest. The Mach number distribution is shown in Figure 12.

Figure 12. Mach-number distribution over cascade at $C_p = -2.5$
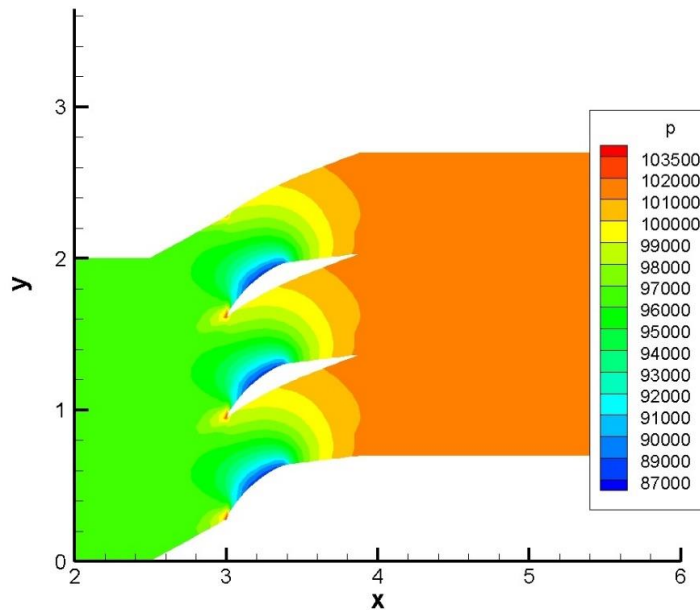
Test Scenario $C_p = -2.1$
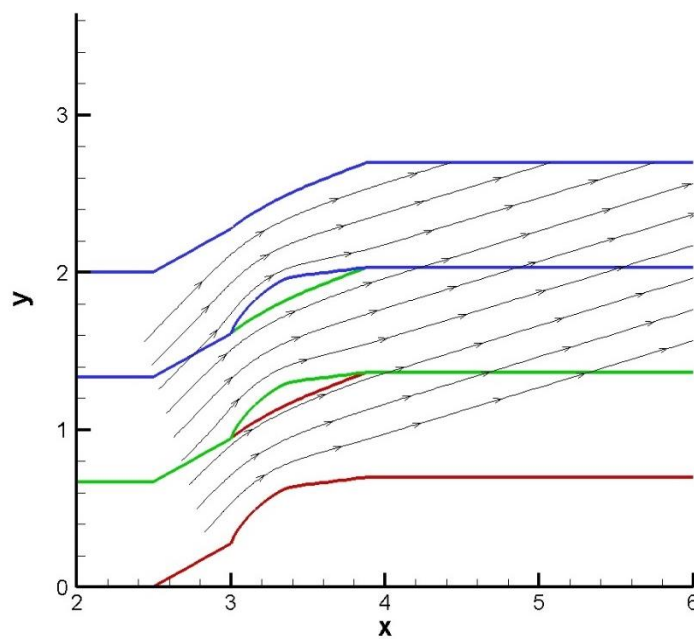
Figure 13. Streamline distribution over cascade at $C_p = -2.1$

Concerning the simulation results at $C_p = -2.1$, the flow suffers from a larger diversion than in the previous case. The flow angle from the axial direction is 16.59° (see Figure 13).

Figure 14. Pressure distribution over cascade at $C_p = -2.1$

With the optimal pressure distribution (the largest area below the pressure distribution curve) the flow has the maximum deflection. The mass flow rate is $113.45 kg/s^2/m$. The pressure increment is the largest from the investigated scenarios (see Figure 14). The inlet static pressure is $p_{in} = 96,366 \, Pa$. The pressure rise in this case is $\pi = 1.0508$. The low pressure zone on the suction side is slightly larger than in the previous case because the pressure increment starts later. The Mach number distribution is found in Figure 15.
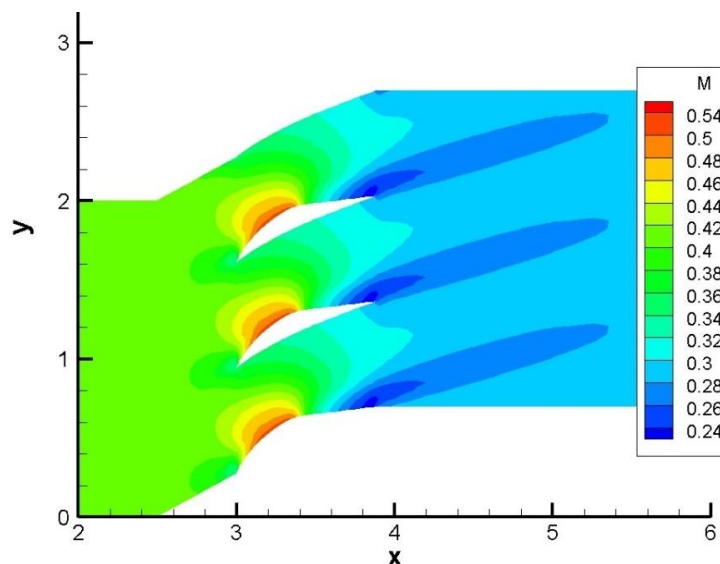
Figure 15. Mach-number distribution over cascade at $C_p = -2.1$

The Effect of Blade Pitch

In this subchapter the effect of the distance between the profiles will be investigated. Because of the large area between the blades in Fig. 7, the flow can pass the blades without major diversion and to achieve higher static pressure rise, the blade profiles has to thicken. The distance

between the profiles will be reduced to determine the consequence and find the most effective distance. The distance is normalized value in connection with the chord.

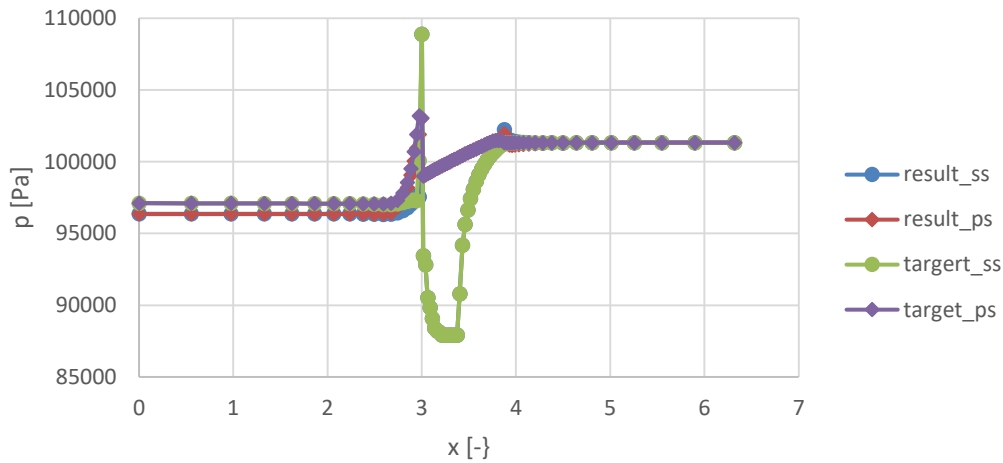*The Initial Blade Distance: Δy = 0.667, C_p = −2.1*

Figure 16. Pressure distribution at the initial blade distance

The properties of this design have been discussed in the previous chapter. The pressure distribution belongs to the $C_p = -2.1$ is shown in Figure 16. The pressure distribution determined by Stratford's method shows great similarity with the results gained after the inverse design. The inverse design method works as expected. As said in a previous chapter the Reynolds number must be in the range of *10E6*. In this case the *Re = 5.226E6* which is in the limits.

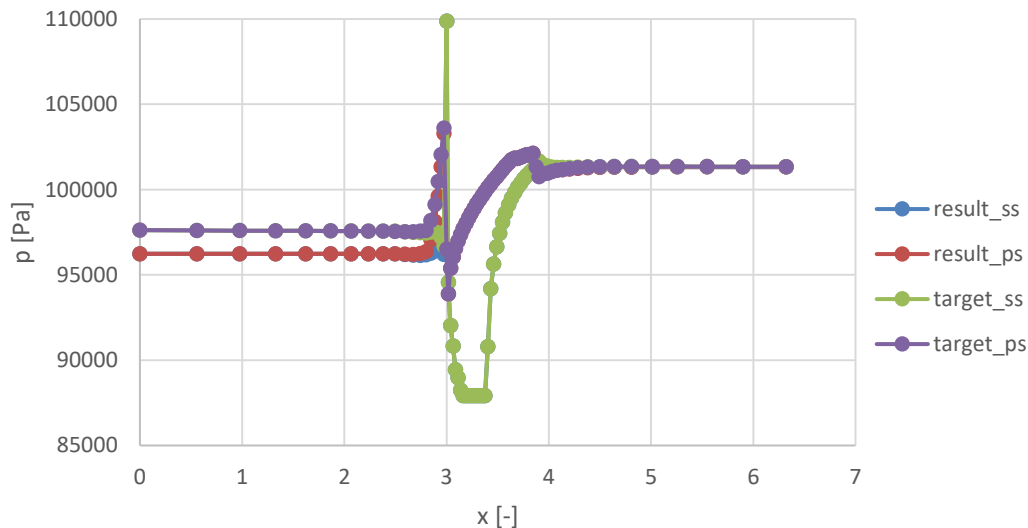*Blade distance is Δy = 0.517, C_p = −2.1*

Figure 17. Pressure distribution at 22.5% narrowed cascade

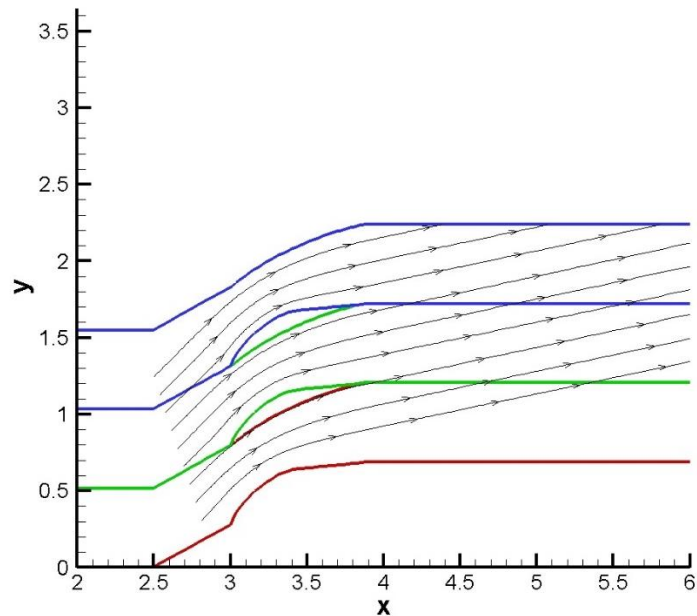The distance is reduced by 22.5% to investigate the effect of narrowed flow section.

Figure 18. Streamlines at 22.5% narrowed cascade

With narrowed flow section the mass flow also slightly increased $113.74\ kg\,/\,s^2\,/\,m$. The blade geometry is slightly changed to adapt better to the target pressure distribution. The rear part becomes more axial. The angle of the flow from the axial direction is 11.88° (see Figure 18).
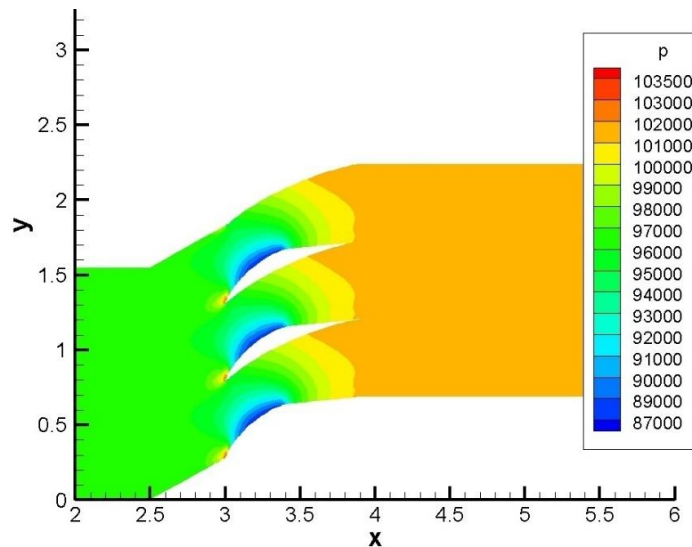

Figure 19. Pressure distribution at 22.5% narrowed cascade

The pressure increase is also improved (see Figure 19). The inlet pressure $p_{in} = 96{,}233\,Pa$ The static pressure rise is $\pi = 1.053$, which is a minimal difference in comparison.
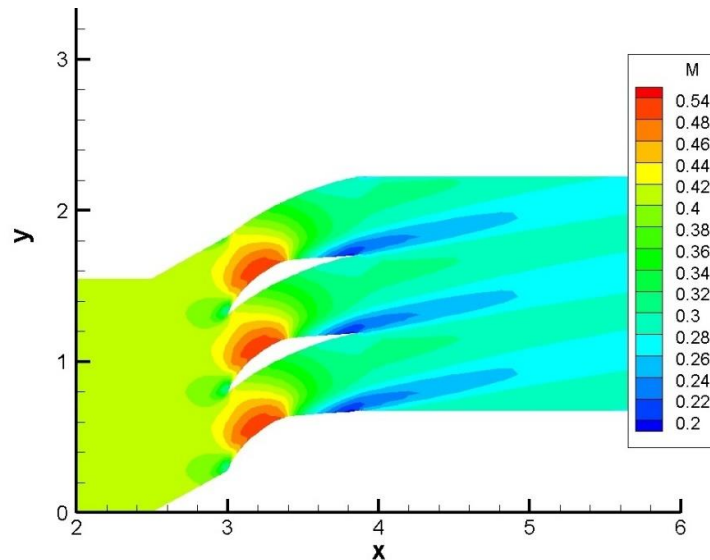
Figure 20. Mach-number distribution at 22.5% narrowed cascades

The Mach-number reduced slightly over the profiles (see Figure 20).

The further pitch reduction with $\Delta y = 0.367$ showed unexpected blade shape, so it is not presented here.

However, it can be concluded that there is a certain blade pitch which, together with the inverse design method, provides the maximal flow turning, mass flow rate and static pressure rise at the given boundary conditions.

CONCLUSION

An inverse design based optimization method has been used and tested in the present case for determining the suction side profile of a blade in a cascade corresponds to the maximal flow turning in axial direction, the maximal mass flow rates and the maximal static pressure rise. The applied DASFLOW software has been developed at BME, Department of Aeronautics, Naval Architecture and Railway Vehicles.

At the start of the investigation an initial profile had to be considered, which will make up the cascade. For this purpose the NACA 65-(18)10 profile [11] has been used.

The second step was to determine a suction side pressure distribution, which is close, but certain safe distance far from the separation in case of positive pressure gradient. Stratford's separation prediction method was used to determine the pressure distribution. This method was implemented in an Excel table. The required pressure distributions belong to different flow conditions are determined by the table.

The next step was to run the inverse design solver with expected pressure distributions for the profile at different pressure coefficients.

The program with initial blade pitch was executed with three pressure coefficients. The one of them is with the largest area under the curve ($C_p = -2.1$). The other two were the curves with minimum area below the pressure distribution ($C_p = -1.6$ and -2.5). The results show that with

increasing of the pressure coefficient starting from its the minimal value, the largest static pressure rise and mass flow rate can be achieved at the optimal value. The flow turning into the axial direction is also the highest one in this case. The pressure coefficient ($C_p = -2.1$) belongs to that conditions.

The effect of the blade pitch (narrowed flow section) was also investigated with the same method as mentioned above. The results showed that with the decreasing of the distance between the profiles there should be an optimum, where the flow turning into the axial direction, the mass flow rate and static pressure rise are the highest ones.

It is important to mention that the profiles were only investigated from fluid mechanics point of view, the mechanical stress analysis requires further work.

The inverse design method can be used to find an optimum design - belongs to the application range of the method - which satisfies the most expected conditions (mass flow rate, static pressure rise and flow turning) in the present case. However, in that case other properties of the profile can deteriorate.

For this work the goal was to combine a separation prediction method with an inverse design method. This is achieved and the flow behaviour is understood. To utilize the results of the present investigation in the development of improved cascades the behaviour of the flow and the interaction between the flow and surface must be understood deeper. The presently used method can be improved further with the extension to compressible and viscous flow. In the future the method can be combined with 3D modelling software to automatically make a blade, which can be investigated by CAE software.

REFERENCES

[1] K. Beneda: Numerical Simulation of MEMS-based Blade Load Distribution Control in Centrifugal Compressor Surge Suppression, Seenith Sivasundaram (ed.) ICNPAA 2012 Congress: Mathematical Problems in Engineering, Aerospace and Sciences, American Institute of Physics, pp. 116-123.

[2] J. Schweighofer, K. van der Meij, A. Gronarz, Cs. Hargitai, Gy. Simongáti: Demonstration by simulation: The four simulator demonstrators of the FP7 EU project MoVeIT!, Proceedings of Hydrodynamics and simulation applied to Inland Waterways and Port Approaches Conference, Paris: Societe Hydrotechnique de France, Paper Schweighofer et al. ISBN:979-10-93567-08-2, p. 10.

[3] J. Bera, L. Pokorádi: Monte-Carlo Simulation of Helicopter Noise, Acta Polytechnica Hungarica, 12:(2) pp. 21-32, 2015.

[4] D. Rohács, J. Rohács: Magnetic levitation assisted aircraft take-off and landing Progress in Aerospace Sciences, 85: pp. 33-50, 2016.

[5] Á. Veress: Bevezetés az áramlástan numerikus módszereibe, Budapesti Műszaki és Gazdaságtudományi Egyetem, tanszéki oktatási segédlet, Budapest, (online) url: http://www.vrht.bme.hu/letoltes/Tanszeki_letoltheto_anyagok/Oktatok_anyagai/Dr.Veress_Arpad_anyagai/Oktatott_targyak/Bevezetes_a_numerikus_aramlastanba_CFD/CFD-jegyzet.pdf, (15.03.2017)

[6] Á. Veress and J. Rohács: Application of Finite Volume Method in Fluid Dynamics and Inverse Design Based Optimization, Computer and Information Science - Numerical Analysis and Scientific Computing - "Finite Volume Method - Powerful Means of Engineering Design", ISBN 978-953-51-0445-2, pp. 3-34, (online) url: http://www.intechopen.com/books/finite-volume-method-powerful-means-of-engineering-design/application-of-finite-volume-method-in-fluid-dynamics-and-inverse-design-based-optimization, (15.03.2017)

[7] Á. Veress, T. Gallina, J. Rohács: Fast and Robust Inverse Design Method for Internal and Cascade Flows, International Review of Aerospace Engineering, Vol. 3 Issue 1, p41, 2010.

[8] S. Eivind: Design of Airfoil for downwind wind turbine Rotor, Norwegian University of Science and Technology, (online) url: https://daim.idi.ntnu.no/masteroppgaver/004/4591/masteroppgave.pdf, (15.01.2017)

[9] C. B. Laney: Computational Gasdynamics, Cambridge University Press, 1998. (online) url: https://books.google.hu/books?hl=hu&lr=&id=r-bYw-JjKGAC&oi=fnd&pg=PP1&dq   =C.+B.+Laney,+Computational+Gas+Dynamics,+Cambridge+University+Press,+1998.&ots=jVnDKtw28l&sig=czS9gixtrGu5sRqtZ-WWuSnUmhc&redir_esc=y#v=onepage&q&f=false,(15.03.2017)

[10] Barth and M. Ohlberger: Finite volume methods: foundation and analysis, (online) url: http://citeseerx.ist.psu.edu/viewdoc/download?doi=10.1.1.6.403&rep=rep1&type=pdf, (15.03.2017)

[11] Seymour M. Bogdonoff, Harriet E. Bogdonoff: Blade design data for axial-flow fans and compressors, p. 23, (online) url: http://digital.library.unt.edu/ark:/67531/metadc62634/m1/23/ (15.03.2017).

[12] A. M. O. Smith: High-Lift Aerodynamics, Journal of Aircraft, Vol. 12 No. 6, pp. 501-530, 1975.

[13] P. Parragi: Inverz tervezési módszer alkalmazási lehetőségének vizsgálata lapátrácsban statikus nyomásnövelés érdekében, MSc diplomaterv, BME, Vasúti Járművek,Repülőgépek és Hajók Tanszék, 2013.

[14] W. Sutherland: The viscosity of gases and molecular force, Philosophical Magazine, S. 5, 36, pp. 507-531, 1893.

INVERZ TERVEZŐELJÁRÁS ALKALMAZÁSA LAPÁTRÁCSOK STATIKUS NYOMÁS NÖVELÉSE CÉLJÁBÓL

Napjainkban a számítógéppel támogatott mérnöki tevékenységbe tartozó módszerek növekvő tudományági lefedettsége és elterjedése figyelhető meg az ipar minden területén. Ennek oka, hogy a szimulációk által segített folyamat- és terméktervezés alkalmazásával jelentős idő-, költség- és kapacitás-csökkenés érhető el. A CAE egyik összetevője a CFD, amelynek hatékonyságát optimalizációs algoritmusokkal lehet tovább javítani. Egy ilyen technológia az inverz tervező eljárás, amelyben egy előre definiált, feltételek figyelembevételével alakítja ki az elvárt geometriát. A BME, Vasúti járművek, Repülőgépek és Hajók Tanszék által fejlesztett inverz tervező program segítségével azt vizsgáltam, hogy egy lapátrácsban, adott belépő torlóponti nyomás, hőmérséklet és áramlás-irány, valamint kilépő statikus nyomás esetén a lapát szívott oldalán milyen leválás-közeli nyomáseloszlás esetén érhető el maximális nyomásnövekedés, axiális irányeltérítés és tömegáram. Munkám során kitértem annak vizsgálatára is, hogy az áramlási keresztmetszet szűkítése miként befolyásolja a vizsgált paramétereket.

Kulcsszavak: numerikus áramlástan, inverz tervező módszer, leválás, optimalizáció, lapátrács

Molnár Dávid (BSc)	Molnár Dávid (BSc)
Hallgató	Student
Budapest Műszaki és Gazdaságtudományi Egyetem	Budapest University of Technology and Economics
Közlekedésmérnöki és Járműmérnöki Kar	Faculty of Transporting Engineering and Vehicle Engineering
Vasúti Járművek, Repülőgépek és Hajók Tanszék	Department of Aeronautical, Naval Architecture and Railway Vehicles
molnarpdavid@gmail.com	molnarpdavid@gmail.com
orcid.org/0000-0002-2384-1836	orcid.org/0000-0002-2384-1836
Dr. Veress Árpád	Dr. Veress Árpád
Egyetemi Docens	Associate Professor
Budapest Műszaki és Gazdaságtudományi Egyetem	Budapest University of Technology and Economics
Közlekedésmérnöki és Járműmérnöki Kar	Faculty of Transporting Engineering and Vehicle Engineering
Vasúti Járművek, Repülőgépek és Hajók Tanszék	Department of Aeronautical, Naval Architecture and Railway Vehicles
averess@vrht.bme.hu	averess@vrht.bme.hu
orcid.org/0000-0002-1983-2494	orcid.org/0000-0002-1983-2494

http://www.repulestudomany.hu/folyoirat/2017_1/2017-1-10-0380_Molnar_David-Veress_Arpad.pdf